ESTIMATION OF ABSORBED DOSES TO TARGET AND HEALTHY TISSUES DURING CONE-BEAM CT RADIOTHERAPY IMAGING OF THE CHEST

M. MARJANOVIĆ[1,2], Á. TÓTH[1,3], B. PETROVIĆ[1,2], I. GENCEL[1]

[1] Radiotherapy Department, Oncology Institute of Vojvodina, Put dr Goldmana 4, 21204 Sremska Kamenica, Serbia
E-mail: marjanovic.milana@onk.ns.ac.rs, *E-mail*: tot.arpad@onk.ns.ac.rs, *E-mail*: petrovic.borislava@onk.ns.ac.rs, *E-mail*: gencel.ivan@onk.ns.ac.rs
[2] Department of Physics, Faculty of Sciences, University of Novi Sad, Trg Dositeja Obradovića 3, 21000 Novi Sad, Serbia
[3] Vinča Institute of Nuclear Sciences, Mike Petrovića Alasa 12–14, 11351 Vinča, Belgrade, Serbia

Received July 19, 2021

Abstract. The aim of this study was to assess volumetric imaging dose and image quality during radiotherapy in case of Hodgkin lymphoma. The absorbed doses were measured using ionization chamber in thorax phantom. For the same setup, Monte Carlo simulations were performed. The image quality was assessed using Catphan phantom. The absorbed doses ranged from 4.4–7.7 mGy (full rotation) and 1.1–3 mGy (partial rotation). Doses from simulation ranged from 6.8–15.6 mGy (full rotation) and 1.9–10.4 mGy (partial rotation). The image quality tests have shown differences between clinical protocols. The imaging doses were smaller than prescribed doses, but shouldn't be neglected.

Key words: *Cone-Beam CT* (CBCT), *Image-Guided Radiation Therapy* (IGRT), *Monte Carlo Method*.

1. INTRODUCTION

The *image-guided radiation therapy* (IGRT) is a procedure that enables conduction of advanced treatments techniques such as IMRT and VMAT, with dose escalation. The success of these techniques heavily relies on accuracy and precision of imaging system. The quality assurance of IGRT system used for patient positioning should be done according to international guidelines [1, 2, 3]. However, repeated usage of X-ray imaging may result in possibly significant additional dose to the patient. The final step in implementation of IGRT should include development of site specific imaging protocols, balancing the clinical benefits of imaging against the expected dose to the patient, which is linked to image quality [2, 4].

Since radiotherapy is the most effective single modality for local control of Hodgkin lymphoma, the present study focused on population of Hodgkin lymphoma patients, usually younger with long post-treatment life expectancies. Consequently,

the additional dose from IGRT may be important in treatment of those patients. The aims of the study were two folded: first aim was to quantify doses to the target, heart, lung and spinal cord from different kV cone beam CT (CBCT) thorax scan protocols using CIRS thorax phantom and MC simulations for the same setup and to quantify image quality of these kV CBCT protocols using Catphan phantom. Monte Carlo is the most accurate method for dosimetric calculations, therefore it is ideal tool to evaluate the delivered dose from CBCT unit [5]. The second aim of this study was to find appropriate protocol of CBCT acquisitions in order to optimize image guidance and limit dose to the patients from kV CBCT systems. As kV CBCT modality is new at our institution and in Serbia in general, this work was the first step to provide guidance for clinicians and help them in decision making when prescribing imaging to a patient.

2. MATERIAL AND METHODS

2.1. CBCT SYSTEM AND SCANS PARAMETERS

X-ray Volume Imaging is an electronic imaging device designed with a kV X-ray source and flat-panel amorphous silicon detector placed 90° to the gantry axis. XVI can work in four different modes, where only the CBCT mode will be considered here. The calibration, image acquisition, processing and cone-beam CT reconstruction have been provided with one application. This system has several collimator cassettes and two filters. The characteristics of the system used in this work are given in Table 1, together with the scanning parameters measured and evaluated.

Table 1

Scanning parameters of evaluated clinical protocols

Protocol	Chest		Thorax Partial Left		Thorax Partial Right	
Output characteristics	120 kV		120 kV		120 kV	
	264 mAs per acquisition		74 mAs per acquisition		74 mAs per acquisition	
Number of frames	660		370		370	
Filter	F1 (bow-tie)		F1 (bow-tie)		F1 (bow-tie)	
Collimator	M20		S20		S20	
Field projections (width × length)	Asymmetric 27.67 cm × 27.67 cm		Symmetric 27.67 cm × 27.67 cm		Symmetric 27.67 cm × 27.67 cm	
Acquisition length	360º		200º		200º	
Direction	clockwise	counter clockwise	clockwise	counter clockwise	clockwise	counter clockwise
Start-stop angle (kV source)	–270º→270º	270º→–270º	70º→–270º	–270º→70º	–270º→110º	110º→–270º

2.2. PHANTOMS

2.2.1. CIRS thorax phantom

The organ dose delivered from X-ray volume imaging CBCT system was measured using CIRS Thorax phantom and Farmer ionization chamber. The choice of the phantom for this study was based on capability of performance and patient's similarity. The CIRS thorax 002 LFC phantom was extensively used in other clinical studies and is proven to be appropriate as human torso replacement [6, 7]. The phantom is made of tissue equivalent materials and it contains 10 interchangeable rod inserts for an ionization chamber.

2.2.2. Catphan phantom

The image quality of X-ray volume imaging CBCT system was evaluated using Catphan phantom. The Catphan phantom 503 is a cylindrical image QA phantom, containing three test modules with geometrical structures to test various image quality parameters.

2.3. MEASUREMENT

2.3.1. Doses for target and organs at risk

The phantom was positioned according to clinical positioning protocol for the chest anatomical region. The measurements were performed with calibrated Farmer ionization chamber and Dose 1 electrometer. The chamber was calibrated in terms of air kerma in air at kV CBCT qualities and in terms of absorbed dose to water. Readings were converted to the absorbed dose-to-water in a point according to next equation [8]:

$$D_{w,Q}=M_Q N_{K,Q} P_{Q,cham} P_{sheath} [(\mu_{en}/\rho)_{air}^{w}]_w \quad (1)$$

where M_Q is the leakage-corrected chamber reading in Coulombs and corrected for the influence quantities temperature and pressure, polarity, and electrometer calibration. $N_{K,Q}$ is the air kerma calibration factor for the given beam quality. $P_{Q,cham}$ is the overall perturbation chamber correction factor. P_{sheath} is the correction for photon absorption and scattering in the waterproofing sleeve. $[(\mu_{en}/\rho)_{air}^{w}]_w$ is the ratio for water-to-air of the mean mass energy-absorption coefficients, averaged over the photon spectrum at the reference point in water in the absence of the chamber. All correction factor are found in literature [8].

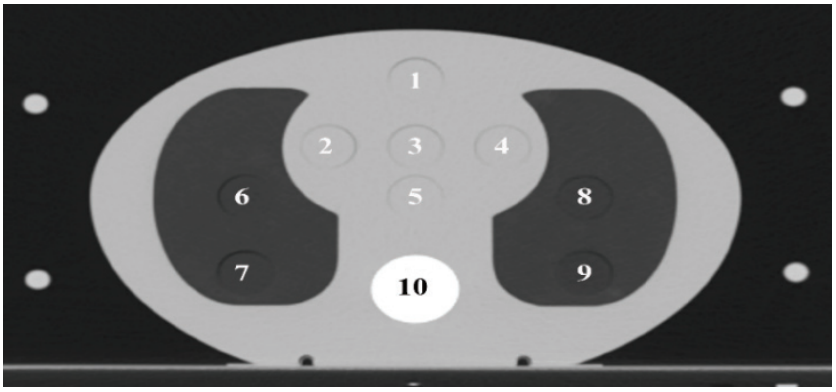

Fig. 1 – Positions of ionization chamber in CIRS thorax phantom.

During the CBCT scans of the phantom all organs inclusive of target were irradiated (heart, both lungs and spinal cord). To measure organ doses, the ionization chamber was inserted in the holes of the phantom. The readings from the Farmer chamber were collected at five points (Fig. 1): 4 – heart, 5 – isocenter, 6 – right lung, 8 – left lung, 10 – spinal cord. Three measurements were averaged in each of those points with scanning protocol listed in Table 1, and mean dose calculated using formula above. The uncertainties were calculated through standards deviation.

2.3.2. Monte Carlo simulations

Monte Carlo (MC) is the most accurate method for dosimetric calculations and is therefore the ideal tool to evaluate the dose delivered by the CBCT unit. In recent years MC codes have been validated in kV energy range [5]. The Elekta XVI CBCT system and phantom was modelled using GEANT4 simulation toolkit. Almost all publications found in literature used voxelised geometries, based on CT scans of phantoms. This method is computational power and time consuming. Therefore, to overcome this problem and check accuracy of the proposed reconstruction, the phantom was reconstructed using *Constructive Solid Geometry* (CSG), since it gives superior performance. All dimensions of phantom and organs were reconstructed using data provided by manufacturer. NIST compound databes materials were used for MC simulations, according to manufacturer specification. Simulation of the X-ray tube is possible in GEANT4, but it is extremely time consuming. External verified X-ray spectra has been used in this work [5] since the full simulation of X-ray tube was not the focus of this paper. F1 bowtie filter was included in MC simulations. All simulations were performed using low energy physics list (EMLivermore), which was recommended in other studies [9, 10, 11]. Number of primaries were estimated to obtain statistical uncertainty below 2%. To verify simulation setup and parameters, comparison of calculated and measured

percentage depth dose curve in water phantom was done. Relative difference between the calculated and measured values was up to 3%.

2.3.3. Image quality

As quality assurance is crucial for IGRT clinical implementation, tests of spatial resolution, uniformity, scale resolution and low-contrast visibility were investigated with Catphan phantom. The Catphan 503 phantom was setup on the treatment couch of the linear accelerator system as recommended. The image quality measurements were performed using scanning parameters listed in Table 1. The measurements were repeated according to acceptance documents (CAT) to check the baseline, with same characteristics as chest scan protocol, except different collimator cassettes S20, S10. After the scans of the Catphan phantom, each module was analysed according to the procedure laid out in the acceptance document of the machine. The reconstruction matrix of clinical protocols has a dimension of 512 × 512, but the reconstruction matrix of CAT has a dimension of 1024 × 1024.

3. RESULTS

3.1. DOSES FOR TARGET AND ORGAN AT RISK

The mean absorbed dose values to all points of interest were measured and calculated under conditions listed in Table 1. The measurements and calculation results were both recorded in Table 2. The impact of kV CBCT source to organs at risk and also for target are small. There was no significant difference in absorbed doses for target and organs at risk between *clockwise* (CW) and *counter clockwise* (CC) protocols. The values found were 2.5–4 times higher for chest protocol than from partial protocols. Using chest protocol, the mean measured absorbed dose per fraction varied from 4.4 mGy to 7.7 mGy and the MC simulations dose range were from 6.79 mGy to 16.99 mGy. Using thorax partial left protocol, the mean measured absorbed dose per fraction varied from 1.8 mGy to 2.5 mGy and for MC simulations dose range were from 1.79 mGy to 8.28 mGy. Using thorax partial right protocol, the mean measured absorbed dose per fraction varied from 1.1 mGy to 3 mGy and for MC simulations dose range were from 2.33 mGy to 3.27 mGy.

For further comparison, when considering radiotherapy of Hodgkin lymphoma prescribed doses were 1.8 Gy per fraction, and imaging has been done for the first three fractions, than once a week. In the worst case scenario, where prescribed dose is 36 Gy in 20 fractions for Hodgkin lymphoma radiotherapy treatment and CBCT scan has been done for each fractions, the contribution of imaging dose to target and OARs were estimated and presented in Figure 2.

Table 2

Measured and calculated absorbed dose for target and organs at risk from different CBCT protocols. Statistical uncertainty for MC simulations was below 2%

Protocol	Chest			Thorax Partial Left			Thorax Partial Right		
Chamber position	CW	CC	MC simulations	CW	CC	MC simulations	CW	CC	MC simulations
	Dose [mGy]								
Heart	7.65±0.26	7.69±0.48	7.90	2.07±0.01	2.10±0.04	1.79	3.01±0.01	2.97±0.11	3.27
Isocenter	6.82±0.27	7.05±0.44	6.79	2.06±0.11	2.01±0.09	2.01	2.40±0.04	2.26±0.01	2.33
Right lung	7.09±0.08	7.09±0.13	8.38	2.29±0.04	2.21±0.04	2.59	2.32±0.05	2.38±0.13	2.65
Left lung	6.65±0.18	6.73±0.16	8.39	2.47±0.04	2.44±0.02	3.13	2.91±0.04	2.75±0.13	3.20
Spinal cord	4.66±0.10	4.38±0.15	16.99	1.84±0.04	1.75±0.07	8.28	1.14±0.08	1.12±0.07	2.63

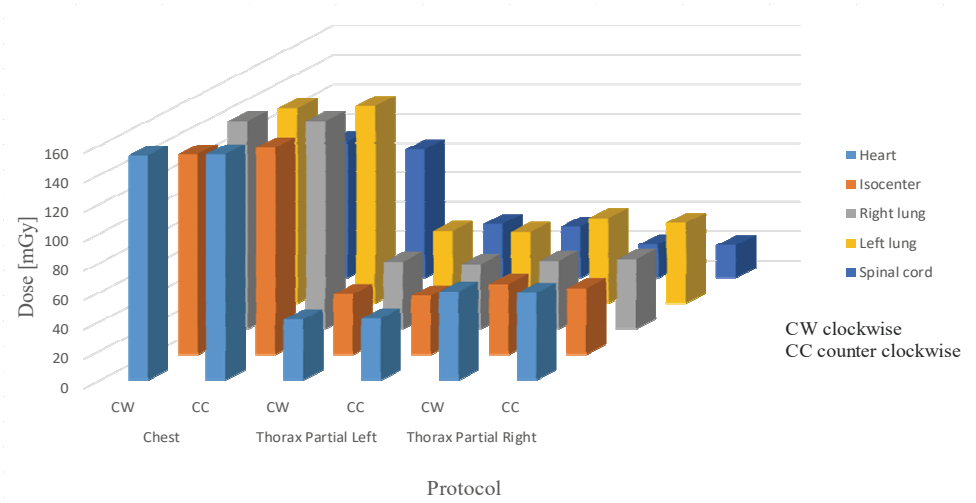

Fig. 2 – (Color online) Target and organs at risk cumulative dose estimation from IGRT to patient with Hodgkin lymphoma.

3.2. IMAGE QUALITY

The results of image quality tests are shown in Table 4. According to Elekta XVI acceptance test specifications, our clinical results indicated that the image spatial resolution and uniformity were very poor and did not meet the required specification of 10 lp/cm and ≤1.5%, respectively, achieved during customer acceptance tests. The low-contrast visibility was the best for chest protocol, since mAs value was the highest compared to partial protocols. For thorax right protocol

the low-contrast visibility was in agreement with specification of <3% as was the result of customer acceptance test. The worst results found were for thorax partial left clockwise protocol. For all protocols, the scale resolution was in agreement with specification of 117 ± 1 mm for lateral and vertical direction and 110 ± 1 mm for longitudinal direction.

For comparison, imaging quality was done for protocols from XVI acceptance test. The *customer acceptance test* (CAT) was in good agreement with Elekta XVI acceptance test specifications for their protocols and for all tests, as it is shown in Table 3.

Table 3

Image quality results from different CBCT protocols

Protocol	Chest		Thorax Partial Left		Thorax Partial Right		CAT
Test	CW	CC	CW	CC	CW	CC	CAT
Uniformity test	2.64%	2.87%	2.36%	2.09%	1.86%	1.84%	0.86%
Low-contrast visibility	1.27%	1.16%	3.07%	2.42%	2.00%	1.50%	2.14%
Spatial resolution [lp/cm]	4	4	4	4	4	4	12
Geometrical resolution:							
lateral direction [mm]	116.0	116.1	116.2	116.2	116.9	116.6	116.8
vertical direction [mm]	116.4	116.1	116.7	116.9	116.9	117.4	116.8
longitudinal direction [mm]	110.1	110.2	111.0	110.1	110.5	110.2	109.9

4. DISCUSSION

In this study, higher doses were measured with chest scan protocol, than from partial scan protocols, which was expected due to acquisition angle. The same dose trend was found in MC simulations. Using chest protocol, the highest values were found for heart and the lowest values were found for spinal cord, with both scan directions. MC simulations agreed well with measured values for heart, isocenter, right lung and left lung the relative difference was 3.3%, 0.5%, 18.2% and 26.2%, respectively.

The major difference between measurements and calculations was found in spine, where dose measured by ionization chamber placed in the spinal insert, was 2.6 times lower than the same calculated by MC simulations. Similar results were found in literature [5, 11, 12, 13]. This can be explained with enhanced dose absorption in bone mineral due to predominance of photoelectric effect which increased the dose deposited in bony structures [12]. This is one of the limitations of MC simulations – the dose was deposited in the volume of spinal structure, taking into account the thickness and attenuation coefficient for spinal cord, surrounded with bone tissue where the attenuation is quite high, it can be easily calculated that the MC dose was 2 times higher than the measured.

The thorax partial left protocols beam direction passes through posterior side of the phantom. The thorax partial right protocols, beam direction passes through

anterior side of the phantom. Due to such angle acquisition, higher dose measured in the spinal cord can be explained with thorax partial left protocol, accordingly higher measured dose to the heart can be explained with thorax partial right protocol. Following the same principle, due to larger angle acquisition on particular side of the phantom, imaging gave more dose to the left lung than for right lung which can be explained with both partial protocols. The smaller rotation arc introduced an asymmetry in dose distribution, which can be used to spare certain regions in the patient as it is reported in few studies [14, 15, 16]. The same dose distribution was confirmed with MC simulations. The difference between measured and calculated dose were for heart 13.5%, isocenter 2.4%, right lung 13.1%, left lung 26.7% and spine 350% for thorax partial left protocols. For the thorax partial right difference were for heart 8.6%, isocenter 2.9%, right lung 14.2%, left lung 10% and for spine 130%. Several studies have spared certain regions through different isocenter positions as it is for one sided lung or breast radiotherapy treatment [17, 18, 14, 19].

Generally, the highest values can be explained with quality of X-ray beam and its pathway through medium to reach the chamber. The lowest values for spinal cord can be explained with attenuation of high-density bone material, because the absorbed dose was measured only in point in the middle of bone insert in the phantom and it was calculated as absorbed dose in water and mass absorption coefficient has not been included. Several studies have reported the smallest dose in spinal cord using thorax scan protocol, as it is in our study [17, 18, 20, 21].

Comparison of our results and previous studies [17, 19, 21, 22, 23, 24], had to start with comparison of tube parameters. The kV CBCT imaging parameters had changed significantly over the last 20 years. The major variation was applied to the tube current-time product (*i.e.* mAs); it is nowadays much lower and is reflected in a lower dose for the patient, for at least one order of magnitude.

Considering a worst-case-cumulative Hodgkin's lymphoma treatment planning of 20 fractions, as it is shown in Figure 2, the imaging dose will be in range 88–154 mGy using chest protocol, 35–50 mGy using thorax partial left protocol and 22–60 mGy using thorax partial right protocol. These values can significantly vary, depending on the number of planned fractions and, in a daily practice, other imaging modes used (kV planar images). According to AAPM TG 180 [25], if the cumulative dose from imaging procedures is expected to exceed 5% of the prescribed target dose, the imaging dose should be considered as part of the total dose. In this study, the cumulative kV CBCT imaging dose has reached level of 0.5% of daily dose. The impact to target and organs at risk should be considered as small but not negligible, as significant amount of normal tissue is irradiated in this process and could increase the probability of stochastic effect such as secondary malignancies, especially in breast cancer [26, 27, 28].

Image quality parameters, namely spatial resolution, low-contrast visibility, scale resolution and uniformity, are of outmost importance for accurate patient setup. In our study, spatial resolution is shown to be very poor for clinical imaging parameters, than in case of the CAT imaging parameters, where smaller matrix size

has been used for clinical scans [29]. Nakahara *et al.* [30] showed that spatial resolution of 4 lp/cm is more consistent over a longer period and it is considered acceptable for clinical protocols. The major differences between clinical and CAT tests were observed in low-contrast visibility, where the best visibility is with chest protocol due to the larger the X-ray tube current-time product leading to highest dose for that protocol. To the contrary, left partial protocols gave worse low-contrast visibility results. The low image contrast can be important issue when choosing an appropriate protocol for the patient. Even with poor low-contrast visibility with partial scan protocols, image quality can be sufficient when bony matching is precise enough.

5. CONCLUSION

Measurements by ionization chamber and MC simulations agreed very well for all organs at risk, except for spinal structure, due to reasons discussed above. Therefore, this will be further investigated in future work. MC simulation can be useful tool for dose to organ prediction, even without full X-ray tube simulation using just verified photon spectra and CGS phantom. In this way simulations are several times faster.

Overall recommendation for young Hodgkin lymphoma patient would be to perform IGRT with kV CBCT imaging. This type of imaging provides volumetric imaging information to clinicians, and correction in volumetric image may be much more important for accurate and precise RT delivery, than the imaging dose delivered. In this case, left partial scan protocols should be used, since smaller amount of imaging dose would be delivered to heart, lungs, and breast [14], due to acquisition angle passing through posterior side of patients.

The conclusion related to the image quality tests would be that these tests should be conducted with clinical protocols, as imaging parameters used for clinical applications differ from those applied in CAT. This might be very much misleading for new users of imaging equipment on linear accelerators. Therefore, manufacturers should modify CAT accordingly to clinical imaging parameters, otherwise CAT with perfect imaging under special conditions which are not clinically relevant, is fully irrelevant for clinical practice.

Acknowledgements. This work was partially supported by the Delvidekert "Kiss" Foundation.

REFERENCES

1. E. E. Klein, J. Hanley, J. Bayouth, F.-F. Yin, W. Simon, S. Dresser, *et al.*, *Med. Phys*. **36**, 4197–212 (2009). https://doi.org/10.1118/1.3190392.
2. J.-P. Bissonnette, P. A. Balter, L. Dong, K. M. Langen, D. M. Lovelock, M. Miften, *et al.*, *Med. Phys*. **39**, 1946–63 (2012). https://doi.org/10.1118/1.3690466.
3. J. D. Fontenot, H. Alkhatib, J. A. Garrett, A. R. Jensen, S. P. McCullough, A. J. Olch, *et al.*, *J Appl. Clin. Med. Phys.* **15**, 3–13 (2014). https://doi.org/10.1120/jacmp.v15i1.4528.

4. International Atomic Energy Agency. *Introduction of Image Guided Radiotherapy into Clinical Practice*, Human Health Reports No 16. Vienna: IAEA; 2019.
5. P. Downes, R. Jarvis, E. Radu, I. Kawrakow, E. Spezi., *Med. Phys*. **36**, 4156–67 (2009). https://doi.org/10.1118/1.3196182.
6. L. Rutonjski, B. Petrovic, M. Baucal, M. Teodorovic, O. Cudic, E. Gershevitsh, *et al.*, *Radiat. Oncol.* **7**, 155. (2012). https://doi.org/10.1186/1748-717X-7-155.
7. E. Gershkevitsh, C. Pesznyak, B. Petrovic, J. Grezdo, K. Chelminski, M. Do Carmo Lopes, *et al.*, *Acta Oncol*. **53**, 628–36 (2014). https://doi.org/10.3109/0284186X.2013.840742.
8. C.-M. Ma, C. W. Coffey, L. A. DeWerd, C. Liu, R. Nath, S. M. Seltzer, *et al.*, *Med. Phys*. **28**, 868–93 (2001). https://doi.org/10.1118/1.1374247.
9. F. Smakens, J. M. Letang, C. Noblet, S. Chiavassa, G. Delpon, N. Freud, *et al.*, *Phys. Med. Biol*. **59**, 7703–15 (2014). https://doi.org/10.1088/0031-9155/59/24/7703.
10. C. Fedon, F. Longo, G. Mettivier, R. Longo, Phys. *Med. Biol*. **60**, 311–23 (2015). https://doi.org/10.1088/0031-9155/60/16/n311.
11. T. E. Marchant, K. D. Joshi, *J. Radiological. Prot*. **37**, 13–30 (2016). https://doi.org/10.1088/1361-6498/37/1/13.
12. P. Alaei, E. Spezi, *Phys. Med*. **31**, 647–58 (2015). https://doi.org/10.1016/j.ejmp.2015.06.003.
13. D. Montanari, E. Scolari, C. Silvestri, Y. J. Graves, H. Yan, L. Cervino, *et al.*, *Phys. Med. Biol*. **59**, 1239–53 (2014). https://doi.org/10.1088/0031-9155/59/5/1239.
14. H. Bahig, É. Roussin, M. Yassa, P. Vavassis, C. Lemaire, L. Archambault, *et al.*, *Pract. Radiat. Oncol*. **5**, e521–9. (2015). https://doi.org/10.1016/j.prro.2015.02.009.
15. S. Ueltzhöffer, P. Zygmanski, J. Hesser, W. Högele, J. Wong, J. R. Bellon, *et al.*, *Med. Phys*. **37**, 2985–98 (2010). https://doi.org/10.1118/1.3432617.
16. A. Quinn, L. Holloway, J. Begg, V. Nelson, P. Metcalfe, *Med. Dosim*. **39**, 190–3. (2014). https://doi.org/10.1016/j.meddos.2013.12.009.
17. A. Arns, M. Blessing, J. Fleckenstein, D. Stsepankou, J. Boda-Heggemann, J. Hesser, *et al.*, *PLoS ONE* **12**, 1–15 (2017). https://doi.org/10.1371/journal.pone.0187710.
18. G. Stelczer, D. Tatai-Szabó, T. Major, N. Mészáros, C. Polgár, J. Pálvölgyi *et al.*, *Phys. Med*. **63**, 70–8 (2019). https://doi.org/10.1016/j.ejmp.2019.05.020.
19. B. Winey, P. Zygmanski, Y. Lyatskaya, *Med. Phys*. **36**, 164–73 (2009). https://doi.org/10.1118/1.3036113.
20. G. X. Ding, D. M. Duggan, C. W. Coffey, *Med. Phys*. **35**, 1135–44 (2008). https://doi.org/10.1118/1.2839096.
21. E. Spezi, P. Downes, R. Jarvis, E. Radu, J. Staffurth, *Int. J. Radiat. Oncol. Biol. Phys*. **83**, 419–26 (2012). https://doi.org/10.1016/j.ijrobp.2011.06.1972.
22. W. Y. Song, S. Kamath, S. Ozawa, S. Al Ani, A. Chvetsov, N. Bhandare, *et al.*, *Med. Phys*. **35**, 480–6 (2008). https://doi.org/10.1118/1.2825619.
23. D. E. Hyer, C. F. Serago, S. Kim, J. G. Li, D. E. Hintenlang, J. Appl. Clin. *Med. Phys*. **11**, 181–97 (2010). https://doi.org/10.1120/jacmp.v11i2.3183.
24. Y.M. Moon, H.J. Kim, D.W. Kwak, Y.R. Kang, M.W. Lee, T.I. Ro, *et al.*, *Nucl. Eng. Technol*. **46**, 255–62 (2014). https://doi.org/10.5516/NET.08.2012.080.
25. G. X. Ding, P. Alaei, B. Curran, R. Flynn, M. Gossman, T. R. Mackie, *et al.*, *Med. Phys*. **45**, e84–e99 (2018). https://doi.org/10.1002/mp.12824.
26. J. Ng, I. Shuryak, *Cancer Manag. Res*. **7**, 1–11 (2014). https://doi.org/10.2147/CMAR.S47220.
27. E. M. Ibrahim, K. M. Abouelkhair, G. A. Kazkaz, O. A. Elmasri, M. Al-Foheidi, *BMC Cancer* **12**, 197 (2012). https://doi.org/10.1186/1471-2407-12-197.
28. N. Veit-Rubin, E. Rapiti, M. Usel, S. Benhamou, V. Vinh-Hung, G. Vlastos, *et al.*, *The Oncologist* **17**, 783–91 (2012). https://doi.org/10.1634/theoncologist.2011-0451.
29. M. Chan, J. Yang, Y. Song, C. Burman, P. Chan, S. Li., *Biomed. Imaging Interv. J*. **7**, e11 (2011). https://doi.org/10.2349/biij.7.2.e11.
30. S. Nakahara, M. Tachibana, Y. Watanabe, *J. Appl. Clin. Med. Phys*. **17**, 211–22 (2016). https://doi.org/10.1120/jacmp.v17i3.6047.